DNA Origami as an *In Vivo* Drug Delivery Vehicle for Cancer Therapy

Qian Zhang,[†,‡,⊥] Qiao Jiang,[§,⊥] Na Li,[§] Luru Dai,[§] Qing Liu,[§] Linlin Song,[§] Jinye Wang,[§] Yaqian Li,[‡] Jie Tian,[†,‡] Baoquan Ding,[§,*] and Yang Du[‡,*]

[†]School of Life Science and Technology, Xidian University, Xi'an 710071, China, and Engineering Research Center of Molecular and Neuro Imaging, Ministry of Education, China, [‡]Key Laboratory of Molecular Imaging, Institute of Automation, Chinese Academy of Sciences, 95 ZhongGuanCun East Road, 100190 Beijing, China, and [§]National Center for NanoScience and Technology, 11 BeiYiTiao, ZhongGuanCun, 100190 Beijing, China. [⊥]These authors contributed equally.

ABSTRACT Many chemotherapeutics used for cancer treatments encounter issues during delivery to tumors *in vivo* and may have high levels of systemic toxicity due to their nonspecific distribution. Various materials have been explored to fabricate nanoparticles as drug carriers to improve delivery efficiency. However, most of these materials suffer from multiple drawbacks, such as limited biocompatibility and inability to engineer spatially addressable surfaces that can be utilized for multifunctional activity. Here, we demonstrate that DNA origami possessed enhanced tumor passive targeting and long-lasting properties at the tumor region. Particularly, the triangle-shaped DNA origami exhibits optimal tumor passive targeting accumulation. The delivery of the known anticancer drug doxorubicin into tumors by self-assembled DNA origami nanostructures was performed, and this approach showed prominent therapeutic efficacy *in vivo*. The DNA origami carriers were prepared through the self-assembly of M13mp18 phage DNA and hundreds of complementary DNA helper strands; the doxorubicin was subsequently noncovalently intercalated into these nanostructures. After conducting fluorescence imaging and safety evaluation, the doxorubicin-containing DNA origami exhibited remarkable antitumor efficacy without observable systemic toxicity in nude mice bearing orthotopic breast tumors labeled with green fluorescent protein. Our results demonstrated the potential of DNA origami nanostructures as innovative platforms for the efficient and safe drug delivery of cancer therapeutics *in vivo*.

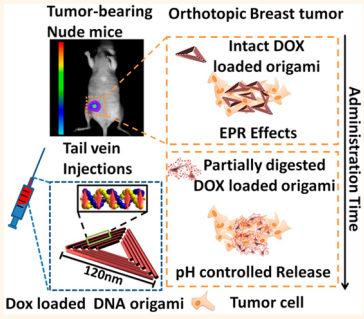

KEYWORDS: DNA origami · doxorubicin · *in vivo* delivery · cancer therapy · fluorescence imaging

Chemotherapy is a standard cancer treatment using cytotoxic antitumor drugs.[1−3] Traditional small molecule chemotherapeutics are nonspecifically distributed in the whole body through blood circulation, which can induce severe systemic toxicity. Despite their widespread use, the poor specificity and limited accumulation of anticancer agents in tumors cause various adverse side effects, such as myelosuppression (depression of the immune system), gastrointestinal distress, alopecia (hair loss), and organ damage; all of these effects can make chemotherapy painful and lead to the failure of the therapy.[1−3] Thus, the development of more effective and safer drugs has been a priority since the initial chemotherapy treatments for cancer in the early 20th century.

In recent decades, various materials, such as self-assembled polymers and metal nanoparticles, have been used to construct nanostructures that facilitate anticancer drug delivery, representing a promising breakthrough in cancer therapy.[4−7] In particular, nanoparticle-based drug delivery systems have demonstrated enhanced permeability and retention (EPR) effects,[5,8] leading to passive drug accumulation in the tumor region. Although considerable effort has been directed to the development of numerous materials as nanocarriers,[4−7,9] the construction of safe, biocompatible, and effective vehicles for drug delivery *in vivo* remains the major challenge for the administration of chemotherapy.[10] Alternatively, structural DNA nanotechnology, especially DNA origami techniques, provides researchers with a robust platform that has potential for novel drug delivery systems.[11−13] With precisely defined nanoscale shapes, uniform sizes, and obvious biocompatibility, self-assembled DNA origami is one of the most promising candidates to serve as the next-generation drug delivery vehicle.[12,13] For DNA origami, a long single strand of DNA (scaffold strand) is folded into arbitrary shapes by hybridizing with hundreds

* Address correspondence to dingbq@nanoctr.cn, yang.du@ia.ac.cn.

Received for review September 24, 2013 and accepted June 25, 2014.

Published online June 25, 2014
10.1021/nn502058j

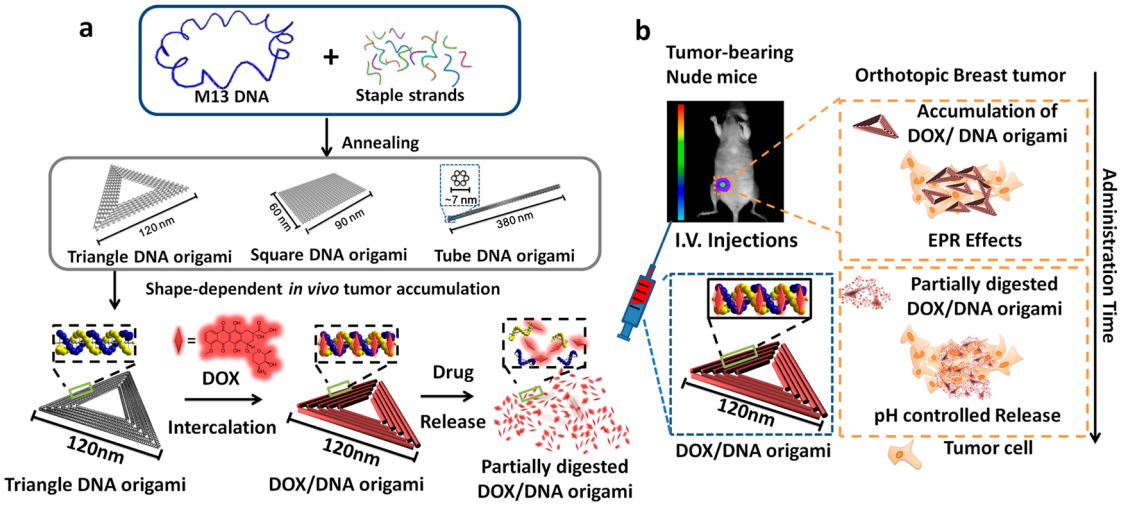

Figure 1. Schematic design of the DNA carrier–drug complex. (a) Long, single-stranded DNA scaffold (M13mp18 phage genomic DNA, blue) hybridizes with rationally designed helper strands to fold into triangular, square, and tube origami shapes. The biodistribution of unstructured M13 DNA and different nanostructures of DNA origami was investigated in subcutaneous breast tumor model. After biodistribution *in vivo*, the triangle-shaped DNA origami demonstrated optimal tumor accumulation; it was then used for doxorubicin intercalation. The Watson–Crick base pairs in the double helices of DNA origami serve as docking sites for doxorubicin intercalation (DOX/DNA origami, red). (b) Tail-injected DOX/DNA origami complexes were delivered *via* blood circulation, accumulating in the breast tumor of nude mice because of EPR effects.

of short DNA strands (helper strands as synthetic oligonucleotides).[11] In addition to maintaining the defined shape of the scaffold, the helper strands can be chemically modified and their unique sequences provide addressable sites for functionalization with various biomolecules and nanoparticles.[14–18] Through these benefits, DNA origami facilitates cellular imaging, targeted payload delivery, and controlled drug release.

Recent studies have indicated that small DNA cages can serve as effective delivery carriers for anticancer drugs, small interfering RNA, immune stimulating CpG oligo-DNA, and antigen molecules, either *in vitro* or *in vivo*.[19–23] Scaffolded DNA origami, which provides enhanced size and controllable shape, can be used to construct multivalent and multifunctional drug carriers as synergetic drug delivery vehicles. DNA origami was found to be stable in cell lysates for 12 h incubation[24] and can be slowly degraded by living cells for 72 h treatment,[25] demonstrating its great potential for controlled drug release. Hexagonal barrel-shaped DNA origami has been used for targeting transport of molecular cargoes, triggered by the activation and reconfiguration of its nanostructure.[26] Furthermore, DNA origami has been used to successfully deliver CpG DNA sequences into spleen cells to test the immune response.[27] Previously, two origami shapes were used to load doxorubicin through intercalation.[28] After administering the drug–origami complex to human breast adenocarcinoma cells (MCF7), the cellular internalization of doxorubicin increased with the aid of DNA nanostructures. The drug–DNA origami complex was effectively transferred into lysosomes through endocytosis at 6 h treatment time. The cytotoxicity of doxorubicin was significantly enhanced against doxorubicin-resistant MCF7 cells by DNA origami carriers.[28] In another doxorubicin–origami delivery system, rational control and tailoring of the drug release kinetics were achieved by designing DNA origami structures. The doxorubicin–origami delivery system also displayed efficient drug transport, resulting in optimal internalization and increased induction of programmed cell death in breast cancer cells.[29] Until now, studies regarding DNA origami as delivery platforms were all performed *in vitro*. Herein, we provide the first evidence that DNA origami can function as a safe drug delivery vehicle for *in vivo* cancer therapy.

In this study, different shapes of DNA origami were assembled, and the structure-dependent tumor accumulating efficiency was investigated. Triangular-shaped DNA origami vehicles were used to load doxorubicin (DOX) through intercalation (Figure 1a). The doxorubicin–DNA origami complexes (DOX/origami) were characterized, and the *in vitro* drug release profiles were evaluated. To examine antitumor effects *in vivo*, drug-loaded DNA origami was administered to nude mice bearing a human MDA-MB-231-GFP orthotopic breast tumor (Figure 1b). Fluorescence imaging, a powerful optical imaging strategy that allows sensitive, longitudinal, and dynamic observation *in vivo*,[30–32] was utilized to investigate tumor growth and drug treatment efficacy. Compared to DOX alone, DOX/origami showed more specific antitumor efficacy without any observable systemic side effects *in vivo*.

RESULTS AND DISCUSSION

DNA Nanocarrier Characterization. The DNA origami nanostructures were assembled using a single-step

annealing process according to Rothemund's and Yan's methods.[11,15] M13 DNA, triangle, tube, and square DNA origami nanostructures were characterized by agarose gel electrophoresis, atomic force microscopy (AFM), and dynamic light scattering (DLS). Different DNA origami nanostructures were successfully assembled as designed (Supporting Information Figure S1). Circular M13 DNA showed wide distribution of hydrodynamic size (radius = 45.7 nm); the triangle DNA origami (radius = 59.0 nm) exhibited a sharp DLS peak, representing uniform hydrodynamic size; the square DNA origami (radius = 80.9 nm) and tube-shaped DNA origami (radius = 98.6 nm) showed wider peaks than triangle DNA origami.

Biodistribution of Different Shapes of DNA Origami. For comprehensively evaluating the structure-dependent tumor accumulating efficiency, we investigated the biodistribution of unstructured M13 DNA and DNA origami with different geometries in a subcutaneous breast tumor model. To visualize the DNA nanostructures *in vivo*, M13 DNA and three DNA origami shapes were designed to incorporate quantum dots (QDs) that exhibited high photon penetration in the animal tissue. The morphological characterization of QD−origami is provided in Supporting Information (Figure S2). MDA-MB-231 subcutaneous tumor-bearing mice were administered with equivalent doses of QDs (5 nM), QD-M13 DNA, QD-triangle origami, QD-tube origami, and QD-square origami (5 nM) *via* intravenous tail injection. Fluorescence imaging was utilized to examine the tumor-targeting effects of QD-labeled DNA structures, and the data were collected at 1, 6, 12, and 24 h after injection. Figure 2a,b shows the dynamic biodistribution of different shape nanostructures labeled with QD *in vivo* during 24 h. Triangle DNA origami nanostructure exhibited the optimal accumulation at the tumor regions compared with square DNA origami and tube DNA origami. The fluorescence signals indicated that the QD-triangle origami accumulated at the tumor site and reached the peak at 6 h ($309.3 \pm 33.1 \times 10^6$ p/s/cm^2/sr) and maintained high levels for 24 h. The QD-tube origami and QD-square origami exhibited relatively high fluorescence signal contrast at the tumor site since 12 h postinjection ($124.3 \pm 10.3 \times 10^6$ and $117.7 \pm 5.0 \times 10^6$ p/s/cm^2/sr, respectively), still lower than that of the QD-triangle origami group. In contrast, the fluorescence signal of the free QD and QD-M13 DNA at tumor sites was weak, and there was no significant difference of fluorescence signals between these two groups. The fluorescence signal of the whole body started to decrease after 1 h and is almost undetected after 24 h postinjection, indicating fast clearance of QD and QD-M13 DNA.

After the fluorescence imaging *in vivo*, the same mice were sacrificed at 24 h postinjection, and the tumor and major organs (brain, tumor, liver, kidney, spleen, lung, and heart) were collected and *ex vivo* fluorescence intensity images were obtained (Figure 2c,d). Compared with QD and unstructured M13 DNA-treated mice, there was obvious stronger fluorescence in tumor tissues of three shapes of DNA origami administration. The *ex vivo* fluorescence imaging results showed that QD-tube origami and QD-square origami was distributed not only in tumor but also in liver and kidney, while the QD-triangle origami was mainly accumulated in tumor and slightly in liver at 24 h (Figure 2c,d). The QD-triangle origami ($392.7 \pm 21.8 \times 10^6$ p/s/cm^2/sr) displayed the highest tumor fluorescence signal compared to QD-tube origami ($299.4 \pm 14.6 \times 10^6$ p/s/cm^2/sr) and QD-square origami ($300.0 \pm 11.5 \times 10^6$ p/s/cm^2/sr); the *ex vivo* result was consistent with the *in vivo* biodistribution, suggesting optimal shape-dependent uptake in the tumor tissues.

The biodistribution results demonstrated that DNA origami possessed enhanced tumor passive targeting and long-lasting properties at the tumor region, which was favorable for improving the antitumor efficacy. Particularly, the triangle-shaped DNA origami exhibits optimal tumor passive targeting accumulation, so the triangle shape was used for subsequent studies of drug loading, intravenous drug delivery in the orthotopic tumor model, as well as safety evaluation.

Drug Loading and Release *in Vitro*. Triangle DNA origami was loaded with doxorubicin, and the drug loading content was measured following our previous reported procedures.[28] After incubating the DNA nanostructures with doxorubicin for 24 h at room temperature, approximately 50% of the drug was loaded in the structures.[28] Morphological characterization of the triangle DNA origami and DOX/origami was conducted using AFM. Each side of the integrated triangular nanostructures was approximately 120 nm long. The AFM images of the triangle DNA origami and DOX/origami provided evidence that the nanostructural morphology was retained after DOX intercalation (Figure S3). The stability of DNA origami and DOX/origami in physiological conditions was investigated. The hydrodynamic radius measurements and gel electrophoresis of DNA origami and DOX/origami demonstrated that there were no obvious structural changes for DNA origami and drug-loaded complexes after 24 h incubation in physiological environment (Figure S3).

Controlled drug release capabilities are critical for drug delivery platforms. Lactic acid is generated due to hypoxia and acidic intracellular organelles inside tumors, lowering the pH values dramatically in tumor regions relative to normal areas;[33,34] these conditions may affect the interaction of drug and DNA nanostructures and facilitate the drug release. Therefore, doxorubicin release from DOX/origami was evaluated in different phosphate-buffered saline (PBS) solutions (pH 5.5 and 7.4). The release profiles were consistent with our previous report.[28] For the first 4 h, <10% of the drug was released from the DNA origami carriers at

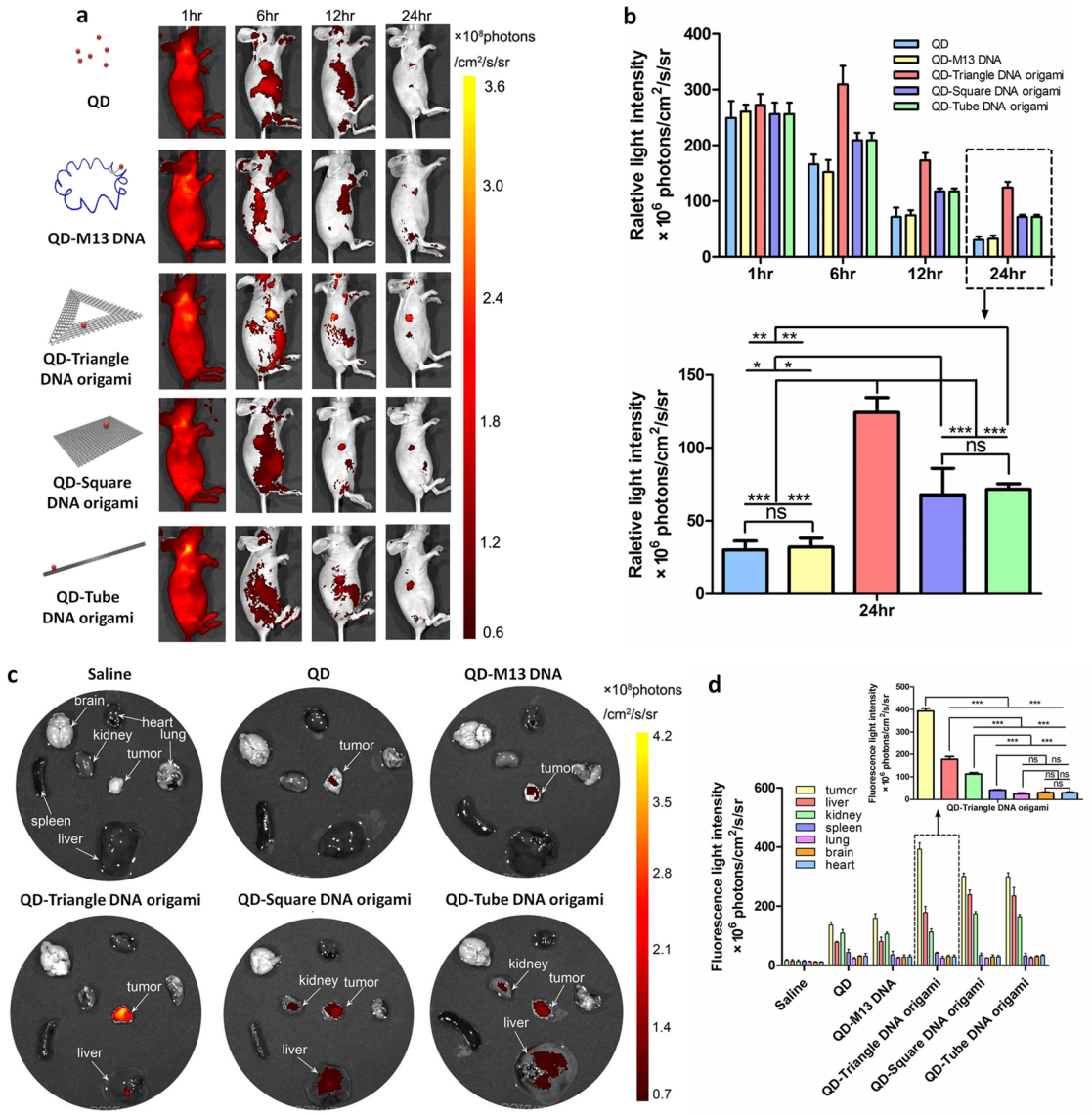

Figure 2. Biodistribution of the DNA origami *in vivo*. (a) Dynamic biodistribution of QD, QD-M13 DNA, QD-triangle DNA origami, QD-tube DNA origami, and QD-square DNA origami monitored in the tumor-bearing nude mice for continuous 24 h through fluorescence imaging. (b) Quantitative analysis of the relative fluorescence light intensity of tumors (ns$P > 0.05$, *$P < 0.05$, **$P < 0.01$, ***$P < 0.0001$). (c) Twenty-four hours after injection, the animals were sacrificed and tumor tissues as well as major organs (brain, tumor, liver, kidney, spleen, lung, and heart) were collected for *ex vivo* imaging. (d) Fluorescence intensities of individual organs from mice treated with different groups. The error bars represent the standard error of the mean of three independent experiments (ns$P > 0.05$, *$P < 0.05$, **$P < 0.01$, ***$P < 0.0001$).

pH 7.4 under physiological conditions. The release process proceeded slowly, reaching ~20% after 48 h. At pH 5.5, similar to the pH of acidic subcellular organelles in tumor cells, the drug release efficiency reached ~35% for the DOX/origami complex (Figure S3). The drug release content was significantly increased when the pH values decreased from 7.4 to 5.5, suggesting that DOX release might be accelerated when DOX/origami was retained in the acidic tumor region and subcellular organelles.

Antitumor Efficacy of Drug-Loaded DNA Origami *in Vitro* and *in Vivo*. The cytotoxicity of DOX and DOX/origami was evaluated using the MDA-MB-231-GFP cell line by the cell-counting kit (cck-8; see Supporting Information for details). From the cell viability assay and fluorescent images, the two groups (DOX and DOX/origami) induced cell death with no significant difference in a concentration range of 0.01 to 100 μM (Figure S4), demonstrating that the DNA origami vehicles delivered the drugs into cancer cells and exhibited antitumor efficacy *in vitro*. A comprehensive evaluation of the antitumor effects of DOX/origami *in vivo* was further performed, and the schematic is shown in Figure 3a. Specifically tumor-bearing mice with tumor volume around 100 mm^3 were randomly divided into four groups (control, DOX, DOX/origami, and origami) for a continuous 12 day treatment. DOX and DOX/origami were injected intravenously at a dose equivalent

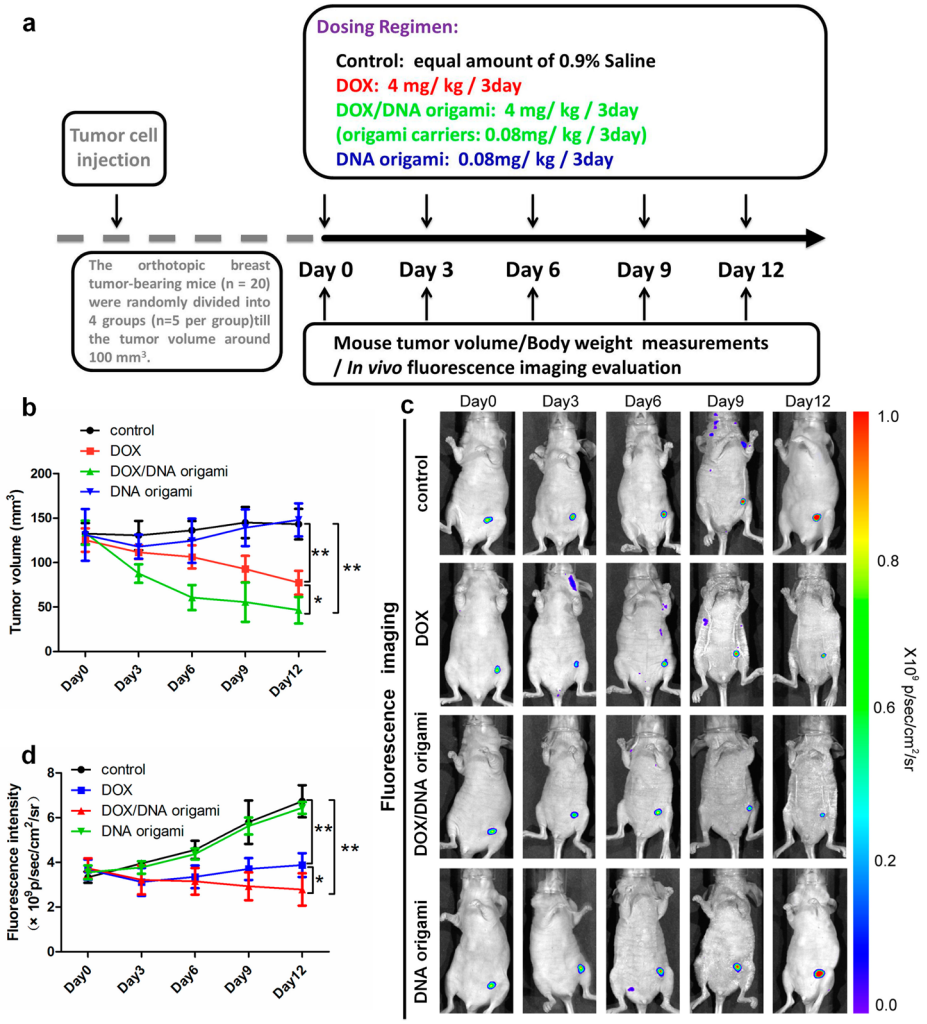

Figure 3. (a) Dosing regimen of the antitumor study. (b) Monitoring tumor growth with different treatments (control, DOX, DOX/DNA origami, and DNA origami) for 12 days. The tumor volumes were measured using a digital calliper every 3 days (volume = $\pi \times a \times b^2/6$, where *a* and *b* are the width and length of the tumors, respectively) (*$P < 0.05$, **$P < 0.01$). (c) *In vivo* real-time fluorescence imaging of the control, DOX, DOX/DNA origami, and DNA origami groups for 12 days. (d) Fluorescence light intensity data analysis for breast-tumor-bearing mice in the control, DOX, DOX/DNA origami, and DNA origami groups for 12 days. The error bars represent the standard error of the mean of three independent experiments (*$P < 0.05$, **$P < 0.01$).

to 4 mg/kg of doxorubicin every 3 days, and the amount of bare origami (0.08 mg/kg/day) was equivalent to the origami in the DOX/origami groups. An equal volume of 0.9% saline was used as a control. The tumor volume was measured after different treatments (Figure 3b). The nude mice treated with DOX and DOX/origami both exhibited tumor volume inhibition effects compared to the saline-treated group, and moreover, the DOX/origami treatment displayed a significantly higher ratio of reducing tumor burden than the DOX-treated group (*$P < 0.05$). No tumor inhibition occurred with the empty DNA origami treatment.

Fluorescence Imaging of Drug-Loaded DNA Origami *in Vivo*. Fluorescence imaging technique is performed in real time and is noninvasive, highly sensitive, and inexpensive.[35,36] With the aid of green fluorescent protein (GFP), the nude mice bearing orthotopic breast tumors derived from the MDA-MB-231-GFP cells displayed strong green fluorescence signal in the tumor regions.

To study the antitumor effects, the fluorescence imaging strategy was utilized to continuously monitor the therapeutic effects of DOX/origami. The fluorescence images were recorded by using the IVIS Imaging Spectrum System, and the data were analyzed using the IVIS Living Imaging 3.0 software (PerkinElmer, USA). In general, the fluorescence signal intensities of the tumor regions continued increasing for the whole 12 day treatment for both the saline and DNA origami treatment, and the two groups of mice exhibited a similar trend. The DOX-treated mice showed slight fluorescence enhancement after 12 day administration. The fluorescence signals were decreased as early as 3 days after treatment with DOX/origami (Figure 3c,d). Furthermore, the average value of the fluorescence light intensities of the DOX/origami

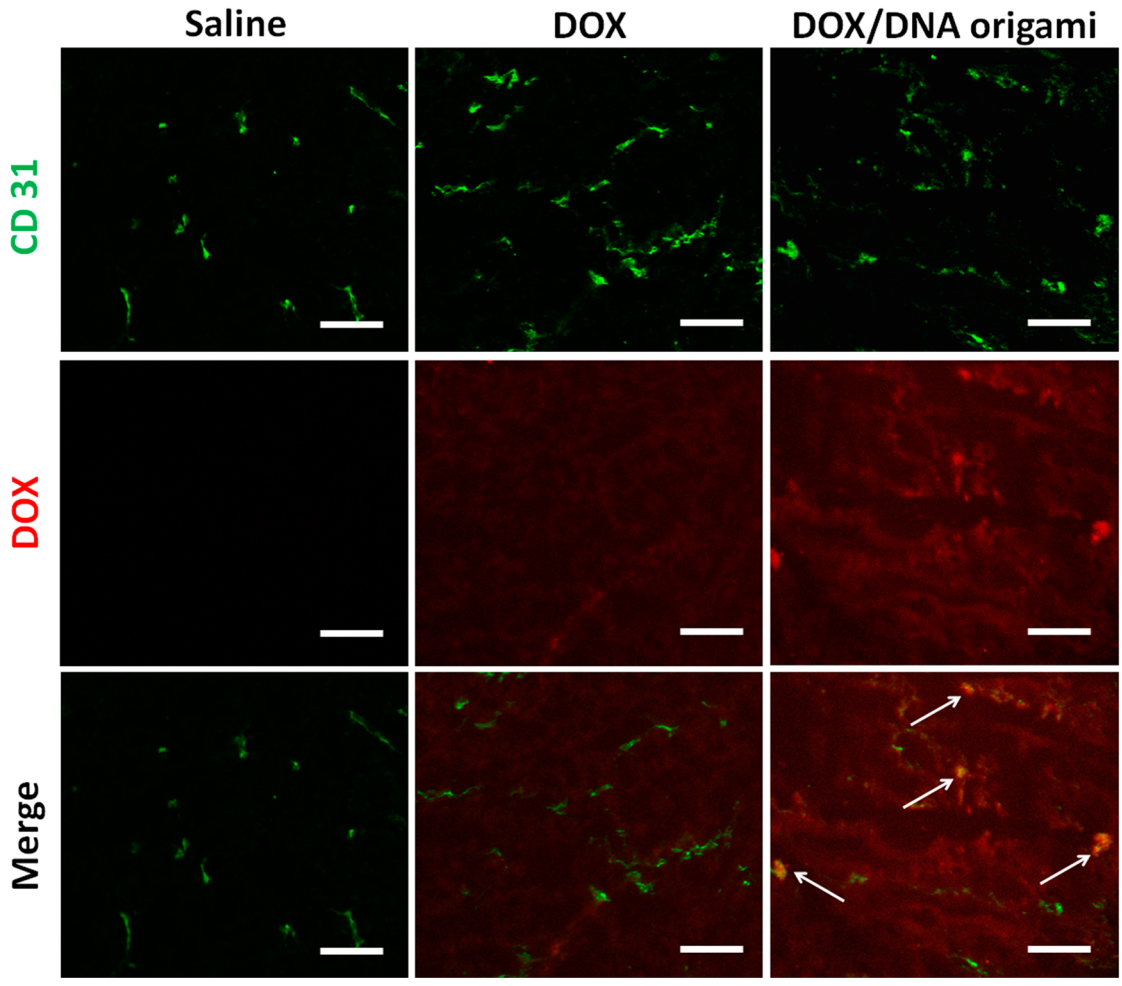

Figure 4. Doxorubicin localization in tumor tissues in relation to the tumor blood vessels detected by the CD31 biomarker. Six hours after the tumor-bearing mice received intravenous injection of DOX, DOX/DNA origami, and saline (control), tumor tissues were frozen, cryosectioned, and stained with CD31. The red fluorescence images of doxorubicin of the tumor tissues and green fluorescence of CD31 were captured under the same slide view (scale bar = 50 μm, 10×, white arrows indicate the drugs delivered by DNA origami distributed surrounding blood vessels).

treatment group ($2.78 \pm 1.25 \times 10^9$ p/s/cm^2/sr) was even less than that of the DOX-treated group ($3.88 \pm 1.19 \times 10^9$ p/s/cm^2/sr) (*$P < 0.05$) on day 12. These results suggested that the DOX/origami delivery system facilitated the antitumor treatment efficacy of doxorubicin *in vivo*, while bare DNA origami did not affect the normal growth of tumor.

Distribution of Doxorubicin within Tumor Tissues. Doxorubicin can be directly visualized (Figure 4) from its own red florescence emission (520−660 nm, two peaks at 550 and 580 nm).[37,38] Therefore, the accumulation of DOX and DOX/origami at the tumor sites can be observed by fluorescence imaging. After administering saline, DOX and DOX/origami, the tumor tissues were collected and cryosectioned for fluorescence examination at 24 h (Leica, Germany). The distribution of doxorubicin in tumor perivascular was assessed by the immunofluorescence (recognized by CD31 antibody, the green fluorescence, Figure 4). The dual color fluorescence of cryosectioned images (Figure 4) showed that there was relatively more doxorubicin at the tumor sites in the DOX/origami-treated group compared with the DOX alone group (Figure 4), and the drug delivered by DNA origami carriers was mainly distributed surrounding blood vessels of tumor regions (Figure 4, indicated by the white arrows). DOX/origami exhibited optimal EPR effects and preferable long-lasting accumulation in the tumor region. By combining passive accumulation with slow drug release *in vitro*, DOX/origami holds the potential to reduce the nonspecific distribution of doxorubicin during the *in vivo* delivery process, inducing controlled drug release in the tumor region.

Systemic Toxicity Studies of Doxorubicin-Loaded DNA Origami Carrier. The safety of DNA nanostructures is critical in the comprehensive evaluation of our DNA origami drug delivery platform. The biocompatibility of the DNA origami's inherent properties as well as any potential influence of the drug delivery process was assessed in the following experiments. The BALB/c mice were treated with the DNA origami carrier and saline individually, and after 6 h, the whole blood and

serum were collected. The whole blood analysis data revealed that the total amounts of white blood cells (WBCs), red blood cells (RBCs), hemoglobin (HGB), and platelet (PLT) were all in normal ranges in the DNA origami-treated group (Table1). The early immunogenic response of DNA origami was monitored by measuring the serum IFN-α level, and the data showed that there was no significant difference between DNA origami-treated and saline-treated mice (Figure 5a). In addition, the effects of DNA origami on the tumor growth, apoptosis, and metastasis-related gene expression was tested on MDA-MB-231 tumor cells. The results demonstrated that DNA origami alone does not affect genes expression regulating tumor growth, apoptosis, or metastasis (Figure S5). Moreover, the total body weight and the histology of the major organs were measured and examined after different treatment for the comprehensive safety assessment. Compared to the saline-treated group, the body weight of tumor-bearing mice did not exhibit significant decrease during the 12 day administration of DOX/origami or origami, while the body weight of the DOX-treated group was significantly decreased (**$P < 0.01$) (Figure 5b). The histological examination of major organs (liver and kidney) in the different treatment groups was examined. The histology of the liver revealed the hepatotoxicity (Figure S6, indicated by the white arrows) in the DOX-treated group but not in the DOX/origami and origami treatment groups.[39−41] The DOX treatment also induced nephrotoxicity (Figure S6, indicated by the white arrows),[42−45] whereas no significant abnormalities were found in the mice treated with saline, DOX/origami, and origami (Figure S6).

TABLE 1. Whole Blood Analysis of White Blood Cell (WBC), Red Blood Cell (RBC), Hemoglobin (HGB), and Platelet (PLT) of DNA Origami and Saline Treatment

blood parameters	control	DNA origami	reference range
WBC ($\times 10^9$/L)	3.1 ± 0.7	4.7 ± 0.8	0.8−6.8
HGB (g/L)	115.2 ± 2.2	112.5 ± 9.1	110−143
RBC ($\times 10^{12}$/L)	7.9 ± 0.2	7.2 ± 0.6	6.36−9.42
PLT ($\times 10^9$/L)	1123.7 ± 218.1	906.7 ± 161.9	450−1590

The orthotopic breast-tumor-bearing nude mice were utilized in this study because they are the preferable animal model for simulating tumor development in human beings. With the help of fluorescence imaging, tumor growth of mice and antitumor efficacy of drug-loaded DNA carriers were dynamically and noninvasively monitored. This noninvasive fluorescence imaging strategy can be utilized to observe the onset and progression of neoplastic transformations. The technique can also be used to visualize and quantify the cellular and physiological processes of tumors *in vivo*, providing obvious advantages over traditional methods, as well as the potential to accelerate the drug discovery process. Furthermore, some antitumor agents usually inhibit tumor progression rather than tumor volume shrinkage. Therefore, the evaluation of therapeutic response only through tumor volume measurement is no longer comprehensive.[46] In our study, both the tumor volume and the fluorescence imaging results revealed that DOX/origami possessed antitumor efficacy without any observable side effects in tumor-bearing nude mice, highlighting the potential of DNA origami as a unique drug carrier for next-generation clinical cancer therapy.

Nanoparticle drug delivery systems with ideal size and controlled three-dimensional (3D) geometry can facilitate passive drug enrichment in the tumor regions using size- and shape-dependent EPR effects.[5,47−49] In our previous study, tubular and triangular DNA origami were used as the nanocarriers for doxorubicin, a chemotherapy drug, and treated MCF7 human breast adenocarcinoma cancer cells.[28] The square-shaped DNA origami binding with virus capsid proteins was used as cellular delivery carrier.[50] So the three particular structures (triangle, tube, and square) were used to investigate shape-dependent DNA origami biodistribution *in vivo*. The *in vivo* biodistribution results (Figure 2) demonstrated that the three DNA origami nanostructures possessed enhanced tumor accumulation and long-lasting properties at the tumor region,

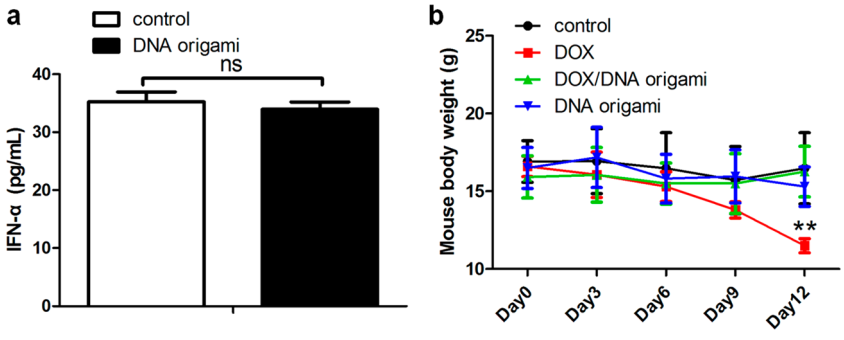

Figure 5. Comprehensive safety assessment for the DNA origami drug delivery platform. (a) Early immunogenic response of DNA origami by measuring the IFN-α level in blood samples. (b) Body weight of the tumor-bearing mice after different treatment was measured every 3 day. The error bars represent the standard error of the mean of three independent experiments ($P < 0.01$).**

which was presumably due to the preferable compactness and size of DNA constructs.[27] Among the three origami structures, the triangle DNA origami exhibited a very sharp DLS peak (Figure S1). The uniform hydrodynamic size of triangle-shaped DNA origami might contribute to the better tumor accumulation effect compared to the square and tube DNA origami. The triangle shape was then used for doxorubicin intercalation, drug delivery *in vivo*, and safety evaluation.

Compared to conventional drug carriers,[51−53] rationally designed DNA nanostructures are safe, biocompatible, and effective drug delivery platforms and are promising candidates for clinical use among numerous nanocarriers (Figure 5, Table 1). Compared to saline treatments, DNA origami did not interfere with normal growth of the tumor (Figure 3), thereby meeting the prerequisites for drug delivery vehicles. Although significant progress has been made using DNA polyhedral wireframe nanostructures as *in vivo* delivery platforms, utilizing programmable DNA origami as *in vivo* antitumor drug carriers has various advantages. Compared to the DNA wireframe cages, the additional layers of tightly packed double helices offer more binding sites per DNA nanostructure for drug intercalation. Therefore, DNA origami can load more doxorubicin than DNA polyhedral wireframe nanocages. The compact origami nanostructures can be loaded with a high concentration of drugs, which are then digested slowly *in vitro* and *in vivo*, offsetting the unintended release of the drug during *in vivo* trafficking. Moreover, the loaded drug was released under low pH values (Figure S3b), which is presumably due to the slow degradation of the DNA nanostructures in the acidic environment. In addition, a change in the ionization state of doxorubicin at low pH could also contribute to the release of drug from the DNA nanostructure. Compared to the uniformly sized DNA cages (approximately 7−20 nm), DNA origami can be designed in sizes ranging from 10 to several hundred nanometers with controlled three-dimensional geometry; this predefined morphology contributes to the significant passive drug accumulation across the tumor vasculature through EPR effects (Figure 4). In our experiment, the triangle-shaped DNA origami exhibits optimal tumor accumulation. The superior EPR effects of DNA origami carriers favored drug accumulation at the tumor site. Therefore, DOX/origami exhibits promising *in vivo* antitumor efficacy (Figure 3) without any observable side effects (Figure 5, Figure S6, and Table 1) due to its size- and shape-dependent EPR effects and its unique drug release properties.

The programmability and addressability of the DNA origami provides a prominent platform for the design and construction of drug vehicles with multiple modifications. The staple strands of DNA origami at controlled sites can be modified precisely with functional groups, such as tumor-targeting peptides, small interfering RNAs, antibodies, and imaging molecules; these functionalities may enable further active tumor-targeting, antitumor efficacy, or *in vivo* imaging functions. Moreover, tumor-targeting biomolecules and/or imaging labeling tags can be organized into one origami template with addressable units. These properties result in the multivalent biological function of the large DNA nanostructures, which are the key features during the construction of multifunctional, active tumor-targeting drug carriers. The interaction between the multifunctional drug carrier and the living organism is multivalent and orientation-dependent, which is difficult to achieve using traditional polymers or metal nanoparticles as the carriers. DNA origami can arrange functional groups with precisely controlled 3D orientations, extending the applications of the self-assembled DNA origami nanostructures within drug discovery and development.

CONCLUSION

We have demonstrated that DNA origami as antitumor drug carriers successfully transported the payloads to tumor regions in nude mice. Through *in vivo* and *ex vivo* imaging, we have confirmed that DNA origami possessed enhanced tumor passive targeting and long-lasting accumulation properties at the tumor region. Particularly, the triangle-shaped DNA origami showed optimal tumor passive targeting accumulation. We further demonstrated that the DNA origami−drug delivery system displayed optimal antitumor efficacy *in vivo* without inducing observable systemic toxicity. Our work demonstrated that DNA origami had great potential in clinical use as efficient and biocompatible antitumor drug delivery platforms.

METHODS

Materials. All oligonucleotides were purchased from Invitrogen (Shanghai, China). The origami staple strands were stored in 1.5 mL Eppendorf tubes with concentrations normalized to 100 μM and were used without further purification. The concentration of each strand was estimated after measuring their UV absorbance at 260 nm. M13mp18 phage single-stranded DNA (N4040S) was purchased from New England Biolabs, Inc. (Beijing, China). Doxorubicin was purchased from Huafeng United Technology (Beijing, China).

Self-Assembly of DNA Origami. DNA origami structures were assembled according to Rothemund's and Yan's work.[11,15] A 1:10 molar ratio between the M13mp18 ssDNA (5 nM) and the short helper strands was used. The DNA origami was annealed and assembled in 1× TAE-Mg^{2+} buffer (Tris, 40 mM; acetic acid, 20 mM; EDTA, 2 mM; magnesium acetate, 12.5 mM; pH 8.0) in an Eppendorf thermocycler (Eppendorf China) by slowly cooling from 90 °C to room temperature over 12 h.

DNA Origami Fluorescent Labeling by QD. One staple strand (C42 for triangle DNA origami and M13 DNA, S34 for squared DNA origami, and T02 for tube DNA origami; see Schemes S1−S3

for details) with biotin modification was assembled into DNA origami (5 nM). Streptavidin-conjugated QD655 (Invitrogen) was then assembled on the DNA template through biotin−streptavidin interaction. The sequence of the biotin-modified strand is

Biotin-C42: 5′-biotin-TTGTAACCGTCTTTCATCAACATTAAAA-TTTTTGTTAAATCA-3′

Biotin-S34: 5′-biotin-TTCGATTTTAGAGGACAGATGAACGGC-GCGACCT-3′

Biotin-T02: 5′-biotin-TTCATCAATTCTACTATTCAAAAGGGT-GAGATAGATTAGAGCCG-3′

Doxorubicin Incorporation into DNA Origami. The drug loading procedure was performed according to our previous work.[28] Briefly, doxorubicin solution (2 mM) was incubated with the triangular DNA origami structures (2.5 nM) for 24 h before being centrifuged at 8000 rpm at room temperature for 10 min. A dark red precipitate (DOX/origami) was then collected. The unloaded doxorubicin in the supernatant was isolated and quantified using UV−vis absorption measurements at 480 nm with a microplate reader (TECAN, Infinite M200, Switzerland). The doxorubicin loading content in the DNA nanocarriers was calculated as demonstrated in a previous report.[28] The details of characterization of DOX/origami and drug release *in vitro* are in the Supporting Information.

Cell Culture. MDA-MB-231 and MDA-MB-231-GFP which are human mammary gland adenocarcinoma cell lines, were procured from the Department of Radiology, Peking Union Medical College Hospital. The cells were labeled with green fluorescent protein using a standard stable transfection protocol. The cells were cultured in Dulbecco's modified Eagle medium (Hyclone, Thermo Scientific), supplemented with 10% fetal bovine serum (Hyclone, Thermo Scientific). The cells were cultured in a 5% CO_2 atmosphere at 37 °C.

MDA-MB-231 Subcutaneous and MDA-MB-231-GFP Orthotopic Tumor-Bearing Mice Model. Athymic female BALB/c nude mice (5−6 weeks old) were purchased from the Department of Experimental Animals, Peking University Health Science Center. All animal experiments were performed in accordance with the guidelines of the Institutional Animal Care and Use Committee at Peking University. The subcutaneous tumor model was established by injecting 150 μL of MDA-MB-231 cell suspension (1×10^6 cells/mL) into the right upper flanks of BALB/c nude mice. The orthotopic tumor model was established by injecting 100 μL of MDA-MB-231-GFP cell suspension (1×10^6 cells/mL) into the lower right mammary fat pad of the BALB/c nude mice.

Characterization of the Biodistribution of DNA Origami *in Vivo*. The fluorescence imaging was utilized to examine the tumor-targeting effects of QD-labeled M13 DNA and different shapes of QD-labeled DNA origami. MDA-MB-231 subcutaneous tumor-bearing mice were used and randomly divided into three groups (n = 3 per group). The mice were administered with equivalent doses of saline, QD (5 nM), QD-M13 DNA, QD-triangle origami, QD-square origami, and QD-tube origami (5 nM) *via* tail vein injection. The QD655-labeled M13 DNA and DNA origami were used to visualize the biodistribution *in vivo* for its red fluorescence (emission maxima of ~655 nm) after being excited by a 500 nm laser. Fluorescence imaging was performed using the IVIS Imaging Spectrum System and analyzed by IVIS Living Imaging 3.0 software (PerkinElmer, USA). A QD655 filter set was used for acquiring the fluorescence of QD-M13 DNA, three shapes of QD-labeled origami, and QDs. The *in vivo* data were collected at 1, 6, 12, and 24 h after injection. The fluorescence light intensity of tumors was used as signal of interest, and the fluorescence light intensity of muscle on the same mouse was used as the background. Fluorescence intensity was normalized as photons per centimeter squared per second per steradian (photons/cm^2/s/sr). The tumor relative fluorescence intensity was calculated according to the following formula:

$$\text{relative light intensity} = \text{fluorescence intensity}_{\text{tumor}} - \text{fluorescence intensity}_{\text{muscle}}$$

Twenty-four hours after tail injection, the same animals were sacrificed and the major organs including brain, tumor, liver, kidney, spleen, lung, and heart were collected, and the *ex vivo* fluorescence imaging was carried out.

DOX/Origami and DOX Treatment. The orthotopic breast-tumor-bearing mice (n = 20) were randomly divided into four groups (n = 5 per group) until the tumor volume was around 100 mm^3. DOX/origami and DOX were administered *via* tail vein injections. The doxorubicin dosage in DOX and DOX/origami treatment was 4 mg/kg and was administered every 3 days during the 12 day treatment. The amount of the origami (0.08 mg/kg) was given equivalently to that used for the DOX/origami groups. The control group received an equal amount of 0.9% saline injection (Figure 3a).

Mouse Body Weight and Tumor Volume. The weight of the mice was measured using an electronic balance every 3 days. The tumor volume was measured by using the digital caliper every 3 days and calculated according to the formula $\pi \times a \times b^2/6$, where a and b were the respective length and width of the tumor.

***In Vivo* Fluorescence Imaging of the Orthotopic Tumor Model.** *In vivo* drug evaluation was performed using the IVIS Imaging System Spectrum and analyzed using the IVIS Living Imaging 3.0 software (PerkinElmer, USA). Fluorescence imaging was implemented on the orthotopic tumor mouse models 0, 3, 6, 9, and 12 days after drug treatment. A GFP filter set was used to acquire the tumor fluorescence light. The fluorescence light intensity of the region of interest of the tumor on each mouse from day 0 to day 12 was quantified. Fluorescence emission images were normalized and reported as photons per second per centimeter squared per steradian.

Immunofluorescent Staining of CD31 on Tumor Tissues. Tumor-bearing mice received intravenous administration of DOX and DOX/origami, each at a dose of 4 mg/kg for 24 h. The tumor tissues were frozen, OCT was embedded, and cryosectioning proceeded. After being washed with PBS and fixed in cold acetone for 15 min, the slides were subsequently blocked by 1% normal goat serum at room temperature for 10 min. The cryosections were overlaid with rat anti-mouse CD31 monoclonal antibody (BD Biosciences, USA) at 4 °C overnight. After removal of the primary antibody and washing with PBS, donkey anti-rat Alexa Fluor 488 (Invitrogen, USA) was added and incubated for 1 h at room temperature. The sections were visualized under fluorescence microscope (Leica, Germany).

Whole Blood Analysis and the IFN-α ELISA Assay. The effects of DNA origami on the whole blood cell (including white blood cell, red blood cell, hemoglobin, and platelet) and plasma IFN-α level were tested. Briefly, the 6 week female BALB/c mice were intravenously injected with DNA origami (5 nM) or equal amounts of saline. Six hours after injection, blood samples were collected, and the blood cell analysis was acquired by an Auto Hematology analyzer BC-2800Vet (Mindray, China). Referenced to Lee's work,[22] the plasma IFN-α level was analyzed by an IFN-α ELISA kit (R&D Systems, USA).

Statistical Analysis. One-way analysis of variance (ANOVA) and Tukey multiple comparisons test or Student's t test was used to determine the statistical differences. *P values <0.05, **P values <0.01 and ***P values <0.0001 were considered statistically significant. Statistical analysis was conducted using Prism4.0 (San Diego, CA, USA).

Conflict of Interest: The authors declare no competing financial interest.

Acknowledgment. The authors are grateful for financial support from National Basic Research Program of China (973 Program, 2012CB934000 and 2014CB748600), National Key Basic Research and Development Program of China (973 Program, 2011CB707700), National Natural Science Foundation of China (81227901, 81090272, 21222311, 91127021), and the National Key Technology Support Program under Grant No. 2012BAI23B06. 100-Talent Program of Chinese Academy of Sciences (B.Q.D.), Beijing Natural Science Foundation (2122057, L140008). Chinese Academy of Sciences Fellowship for Young International Scientists (2013Y1GB0005).

Supporting Information Available: Extra figures and microscopy images. This material is available free of charge *via* the Internet at http://pubs.acs.org.

REFERENCES AND NOTES

1. Young, C. W.; Burchenal, J. H. Cancer Chemotherapy. *Annu. Rev. Pharmacol.* **1971**, *11*, 369–386.
2. Carter, S. K.; Slavik, M. Chemotherapy of Cancer. *Annu. Rev. Pharmacol.* **1974**, *14*, 157–183.
3. Chabner, B. A.; Roberts, T. G. Chemotherapy and the War on Cancer. *Nat. Rev. Cancer* **2005**, *5*, 65–72.
4. Petros, R. A.; DeSimone, J. M. Strategies in the Design of Nanoparticles for Therapeutic Applications. *Nat. Rev. Drug Discovery* **2010**, *9*, 615–627.
5. Davis, M. E.; Shin, D. M. Nanoparticle Therapeutics: An Emerging Treatment Modality for Cancer. *Nat. Rev. Drug Discovery* **2008**, *7*, 771–782.
6. Heath, J. R.; Davis, M. E. Nanotechnology and Cancer. *Annu. Rev. Med.* **2008**, *59*, 251–265.
7. Wang, A. Z.; Langer, R.; Farokhzad, O. C. Nanoparticle Delivery of Cancer Drugs. *Annu. Rev. Med.* **2012**, *63*, 185–198.
8. Torchilin, V. Tumor Delivery of Macromolecular Drugs Based on the EPR Effect. *Adv. Drug Delivery Rev.* **2011**, *63*, 131–135.
9. Zhao, F.; Zhao, Y.; Liu, Y.; Chang, X.; Chen, C.; Zhao, Y. Cellular Uptake, Intracellular Trafficking, and Cytotoxicity of Nanomaterials. *Small* **2011**, *7*, 1322–1337.
10. Jain, R. K.; Stylianopoulos, T. Delivering Nanomedicine to Solid Tumors. *Nat. Rev. Clin. Oncol.* **2010**, *7*, 653–664.
11. Rothemund, P. W. Folding DNA To Create Nanoscale Shapes and Patterns. *Nature* **2006**, *440*, 297–302.
12. Pinheiro, A. V.; Han, D.; Shih, W. M.; Yan, H. Challenges and Opportunities for Structural DNA Nanotechnology. *Nat. Nanotechnol.* **2011**, *6*, 763–772.
13. Chhabra, R.; Sharma, J.; Liu, Y.; Rinker, S.; Yan, H. DNA Self-Assembly for Nanomedicine. *Adv. Drug Delivery Rev.* **2010**, *62*, 617–625.
14. Ding, B.; Deng, Z.; Yan, H.; Cabrini, S.; Zuckermann, R. N.; Bokor, J. Gold Nanoparticle Self-Similar Chain Structure Organized by DNA Origami. *J. Am. Chem. Soc.* **2010**, *132*, 3248–3249.
15. Stearns, L. A.; Chhabra, R.; Sharma, J.; Liu, Y.; Petuskey, W. T.; Yan, H.; Chaput, J. C. Template-Directed Nucleation and Growth of Inorganic Nanoparticles on DNA Scaffolds. *Angew. Chem., Int. Ed.* **2009**, *48*, 8494–8496.
16. Pal, S.; Varghese, R.; Deng, Z.; Zhao, Z.; Kumar, A.; Yan, H.; Liu, Y. Site-Specific Synthesis and *In Situ* Immobilization of Fluorescent Silver Nanoclusters on DNA Nanoscaffolds by Use of the Tollens Reaction. *Angew. Chem., Int. Ed.* **2011**, *123*, 4262–4265.
17. Ding, B.; Wu, H.; Xu, W.; Zhao, Z.; Liu, Y.; Yu, H.; Yan, H. Interconnecting Gold Islands with DNA Origami Nanotubes. *Nano Lett.* **2010**, *10*, 5065–5069.
18. Voigt, N. V.; Tørring, T.; Rotaru, A.; Jacobsen, M. F.; Ravnsbæk, J. B.; Subramani, R.; Mamdouh, W.; Kjems, J.; Mokhir, A.; Besenbacher, F.; *et al.* Single-Molecule Chemical Reactions on DNA Origami. *Nat. Nanotechnol* **2010**, *5*, 200–203.
19. Chang, M.; Yang, C.-S.; Huang, D.-M. Aptamer-Conjugated DNA Icosahedral Nanoparticles as a Carrier of Doxorubicin for Cancer Therapy. *ACS Nano* **2011**, *5*, 6156–6163.
20. Li, J.; Pei, H.; Zhu, B.; Liang, L.; Wei, M.; He, Y.; Chen, N.; Li, D.; Huang, Q.; Fan, C. Self-Assembled Multivalent DNA Nanostructures for Noninvasive Intracellular Delivery of Immunostimulatory CpG Oligonucleotides. *ACS Nano* **2011**, *5*, 8783–8789.
21. Bhatia, D.; Surana, S.; Chakraborty, S.; Koushika, S. P.; Krishnan, Y. A Synthetic Icosahedral DNA-Based Host–Cargo Complex for Functional *In Vivo* Imaging. *Nat. Commun.* **2011**, *2*, 339.
22. Lee, H.; Lytton-Jean, A. K.; Chen, Y.; Love, K. T.; Park, A. I.; Karagiannis, E. D.; Sehgal, A.; Querbes, W.; Zurenko, C. S.; Jayaraman, M.; *et al.* Molecularly Self-Assembled Nucleic Acid Nanoparticles for Targeted *In Vivo* SiRNA Delivery. *Nat. Nanotechnol.* **2012**, *7*, 389–393.
23. Liu, X.; Xu, Y.; Yu, T.; Clifford, C.; Liu, Y.; Yan, H.; Chang, Y. A DNA Nanostructure Platform for Directed Assembly of Synthetic Vaccines. *Nano Lett.* **2012**, *12*, 4254–4259.
24. Mei, Q.; Wei, X.; Su, F.; Liu, Y.; Youngbull, C.; Johnson, R.; Lindsay, S.; Yan, H.; Meldrum, D. Stability of DNA Origami Nanoarrays in Cell Lysate. *Nano Lett.* **2011**, *11*, 1477–1482.
25. Shen, X.; Jiang, Q.; Wang, J.; Dai, L.; Zou, G.; Wang, Z. G.; Chen, W. Q.; Jiang, W.; Ding, B. Visualization of the Intracellular Location and Stability of DNA Origami with a Label-Free Fluorescent Probe. *Chem. Commun.* **2012**, *48*, 11301–11303.
26. Douglas, S. M.; Bachelet, I.; Church, G. M. A Logic-Gated Nanorobot for Targeted Transport of Molecular Payloads. *Science* **2012**, *335*, 831–834.
27. Schuller, V. J.; Heidegger, S.; Sandholzer, N.; Nickels, P. C.; Suhartha, N. A.; Endres, S.; Bourquin, C.; Liedl, T. Cellular Immunostimulation by CpG-Sequence-Coated DNA Origami Structures. *ACS Nano* **2011**, *5*, 9696–9702.
28. Jiang, Q.; Song, C.; Nangreave, J.; Liu, X.; Lin, L.; Qiu, D.; Wang, Z.-G.; Zou, G.; Liang, X.; Yan, H. DNA Origami as a Carrier for Circumvention of Drug Resistance. *J. Am. Chem. Soc.* **2012**, *134*, 13396–13403.
29. Zhao, Y. X.; Shaw, A.; Zeng, X.; Benson, E.; Nystrom, A. M.; Hogberg, B. DNA Origami Delivery System for Cancer Therapy with Tunable Release Properties. *ACS Nano* **2012**, *6*, 8684–8691.
30. Rudin, M.; Weissleder, R. Molecular Imaging in Drug Discovery and Development. *Nat. Rev. Drug Discovery* **2003**, *2*, 123–131.
31. Seddon, B. M.; Workman, P. The Role of Functional and Molecular Imaging in Cancer Drug Discovery and Development. *Br. J. Radiol.* **2003**, *76*, S128–138.
32. Zhang, Q.; Du, Y.; Xue, Z.; Chi, C.; Jia, X.; Tian, J. Comprehensive Evaluation of the Anti-angiogenic and Anti-neoplastic Effects of Endostar on Liver Cancer through Optical Molecular Imaging. *PLoS One* **2014**, *9*, e85559.
33. Aryal, S.; Hu, C. M.; Zhang, L. Polymer-Cisplatin Conjugate Nanoparticles for Acid-Responsive Drug Delivery. *ACS Nano* **2010**, *4*, 251–258.
34. Yuan, Q.; Yeudall, W. A.; Yang, H. PEGylated Polyamidoamine Dendrimers with Bis-aryl Hydrazone Linkages for Enhanced Gene Delivery. *Biomacromolecules* **2010**, *11*, 1940–1947.
35. Dimarzio, C. A.; Niedre, M. Pre-clinical Optical Molecular Imaging in the Lung: Technological Challenges and Future Prospects. *J. Thorac. Dis.* **2012**, *4*, 556–557.
36. Chan, L. W.; Wang, Y. N.; Lin, L. Y.; Upton, M. P.; Hwang, J. H.; Pun, S. H. Synthesis and Characterization of Anti-EGFR Fluorescent Nanoparticles for Optical Molecular Imaging. *Bioconjugate Chem.* **2013**, *24*, 167–175.
37. Pigram, W. J.; Fuller, W.; Hamilton, L. D. Stereochemistry of Intercalation: Interaction of Daunomycin with DNA. *Nat. New Biol.* **1972**, *235*, 17–19.
38. Anderson, A. B.; Gergen, J.; Arriaga, E. A. Detection of Doxorubicin and Metabolites in Cell Extracts and in Single Cells by Capillary Electrophoresis with Laser-Induced Fluorescence Detection. *J. Chromatogr. B: Anal. Technol. Biomed. Life Sci.* **2002**, *769*, 97–106.
39. Santos, R. V.; Batista, M. L., Jr.; Caperuto, E. C.; Costa Rosa, L. F. Chronic Supplementation of Creatine and Vitamins C and E Increases Survival and Improves Biochemical Parameters after Doxorubicin Treatment in Rats. *Clin. Exp. Pharmacol. Physiol.* **2007**, *34*, 1294–1299.
40. Chen, Y. H.; Xu, D. X.; Zhao, L.; Wang, H.; Wang, J. P.; Wei, W. Ascorbic Acid Protects against Lipopolysaccharide-Induced Intra-uterine Fetal Death and Intra-uterine Growth Retardation in Mice. *Toxicology* **2006**, *217*, 39–45.
41. Injac, R.; Perse, M.; Obermajer, N.; Djordjevic-Milic, V.; Prijatelj, M.; Djordjevic, A.; Cerar, A.; Strukelj, B. Potential Hepatoprotective Effects of Fullerenol $C_{60}(OH)_{24}$ in Doxorubicin-Induced Hepatotoxicity in Rats with Mammary Carcinomas. *Biomaterials* **2008**, *29*, 3451–3460.
42. Meng, H.; Xue, M.; Xia, T.; Ji, Z.; Tarn, D. Y.; Zink, J. I.; Nel, A. E. Use of Size and a Copolymer Design Feature To Improve the Biodistribution and the Enhanced Permeability and Retention Effect of Doxorubicin-Loaded Mesoporous Silica Nanoparticles in a Murine Xenograft Tumor Model. *ACS Nano* **2011**, *5*, 4131–4144.

43. Nomura, R.; Ishizaki, Y.; Suzuki, K.; Kawasaki, S. Development of Hepatic Steatosis after Pancreatoduodenectomy. *Am. J. Roentgenol.* **2007**, *189*, 1484–1488.
44. Klinger, M.; Eipeldauer, S.; Hacker, S.; Herberger, B.; Tamandl, D.; Dorfmeister, M.; Koelblinger, C.; Gruenberger, B.; Gruenberger, T. Bevacizumab Protects against Sinusoidal Obstruction Syndrome and Does Not Increase Response Rate in Neoadjuvant Xelox/Folfox Therapy of Colorectal Cancer Liver Metastases. *Eur. J. Surg. Oncol.* **2009**, *35*, 515–520.
45. Yagmurca, M.; Erdogan, H.; Iraz, M.; Songur, A.; Ucar, M.; Fadillioglu, E. Caffeic Acid Phenethyl Ester as a Protective Agent against Doxorubicin Nephrotoxicity in Rats. *Clin. Chim. Acta* **2004**, *348*, 27–34.
46. Cai, W.; Gambhir, S. S.; Chen, X. Molecular Imaging of Tumor Vasculature. In *Methods in Enzymology*; Elsevier: Amsterdam, 2008; Vol. 445, pp 141–176, Chapter 7.
47. Chou, L. Y.; Zagorovsky, K.; Chan, W. C. DNA Assembly of Nanoparticle Superstructures for Controlled Biological Delivery and Elimination. *Nat. Nanotechnol.* **2014**, *9*, 148–155.
48. Albanese, A.; Tang, P. S.; Chan, W. C. The Effect of Nanoparticle Size, Shape, and Surface Chemistry on Biological Systems. *Annu. Rev. Biomed. Eng.* **2012**, *14*, 1–16.
49. Farokhzad, O. C.; Langer, R. Impact of Nanotechnology on Drug Delivery. *ACS Nano* **2009**, *3*, 16–20.
50. Mikkila, J.; Eskelinen, A. P.; Niemela, E. H.; Linko, V.; Frilander, M. J.; Torma, P.; Kostiainen, M. A. Virus-Encapsulated DNA Origami Nanostructures for Cellular Delivery. *Nano Lett.* **2014**, *14*, 2196–2200.
51. Allen, T. M.; Mumbengegwi, D. R.; Charrois, G. J. Anti-CD19-Targeted Liposomal Doxorubicin Improves the Therapeutic Efficacy in Murine B-Cell Lymphoma and Ameliorates the Toxicity of Liposomes with Varying Drug Release Rates. *Clin. Cancer Res.* **2005**, *11*, 3567–3573.
52. Bandak, S.; Goren, D.; Horowitz, A.; Tzemach, D.; Gabizon, A. Pharmacological Studies of Cisplatin Encapsulated in Long-Circulating Liposomes in Mouse Tumor Models. *Anticancer Drugs* **1999**, *10*, 911–920.
53. Minelli, C.; Lowe, S. B.; Stevens, M. M. Engineering Nanocomposite Materials for Cancer Therapy. *Small* **2010**, *6*, 2336–2357.